THE MECHANICAL PERFORMANCE OF CARBON FIBRES- ADDRESSING THE ROLE OF MICROSTRUCTURE

Peter Lynch[1, 2], Claudia Creighton[1], David Fox[2], Pablo Mota Santiago[1, 3], Adrian Hawley[3], Stephen Mudie[3]

[1]Deakin University, 75 Pigdons Road, Waurn Ponds, Victoria, 3216, Australia.
[2]CSIRO, Manufacturing, 75 Pigdons Road, Waurn Ponds, Victoria, 3216, Australia.
[3] Australian Synchrotron (ANSTO), 800 Blackburn Road, Clayton, Victoria, 3168, Australia.

ABSTRACT

A new SAXS-WAXS method has been developed at the Australian synchrotron for the structural analysis of carbon fibres. The new technique, referred to as serial SAXS-WAXS fibre scattering is used to map the microstructural properties of single carbon fibres, ranging in diameter from 5 to 8 μm. Based on an automated scanning protocol, a single carbon fibre is mounted in vacuum and aligned relative to the incident X-ray beam. After (automated) alignment points on each monofilament are acquired. In the forward scattering direction both the SAXS and WAXS signal are recorded as a single image to ensure that the fibre scattering cross-section is known precisely. Under these conditions both the size and alignment of the microstructural features from fibre-to-fibre are quantified. Importantly, the graphitic alignment, spacing and apparent crystallite size can be directly related to the macroscopic fibre modulus. In addition, quantitative analysis of the SAXS scattering signal from pores trapped within the fibre provides an indication of macroscopic strength. The utility of these techniques are demonstrated for carbon fibres prepared on the Carbon Nexus single tow line at 3 different carbonization tensions.

1. INTRODUCTION

The majority of commercial carbon fibre grades are derived from polyacrylonitrile (PAN) precursors. Carbon Fibre (CF) reinforced composite materials are being increasingly utilised in aerospace and automotive applications to lightweight structures therefore improving fuel efficiency and range (1).

As illustrated by the schematic in Figure 1, the structure of CF consists of turbostratic 2D graphitic layers that display a preferred orientation relative to the fibre axis (2). This alignment has been closely linked with the fibre modulus based on the uniform stress model (3, 4). At the atomic level, this preferred alignment results in extreme anisotropy caused by the in-plane (covalent) and the out of plane (van der Waals) forces (5). Measurement of the aspect ratio of these nanocrystallite clusters has also recently been shown to control fibre anisotropy (6). Consequently, CF's exhibit extraordinary tensile properties.

Copyright 2019. Used by the Society of the Advancement of Material and Process Engineering with permission.

SAMPE Conference Proceedings. Charlotte, NC, May 20-23, 2019. Society for the Advancement of Material and Process Engineering – North America.

Availability of a microstructural model describing CF tensile strength appears to be a more challenging prospect. Fibre tensile strength is driven on both a macroscopic (flaws, impurities, surface defects) and microstructural level (voids, void size and amorphous structure). At the microstructure level, the Griffith's criterion (7) for onset of failure states the mean material strength is dependent on the structural parameter size, in the case of CF the cluster (crystallite) and/or void size. However, Loidl (8) suggests that for certain fibres the Griffith's formula is not necessarily applicable to CF, as the sensitivity of the structural unit to flaws is expected to be approximately 3 nm. At this nanometre scale, it is was proposed that the arrangement (orientation) of the crystallites and potential for interlinking can play a driving force in failure initiation.

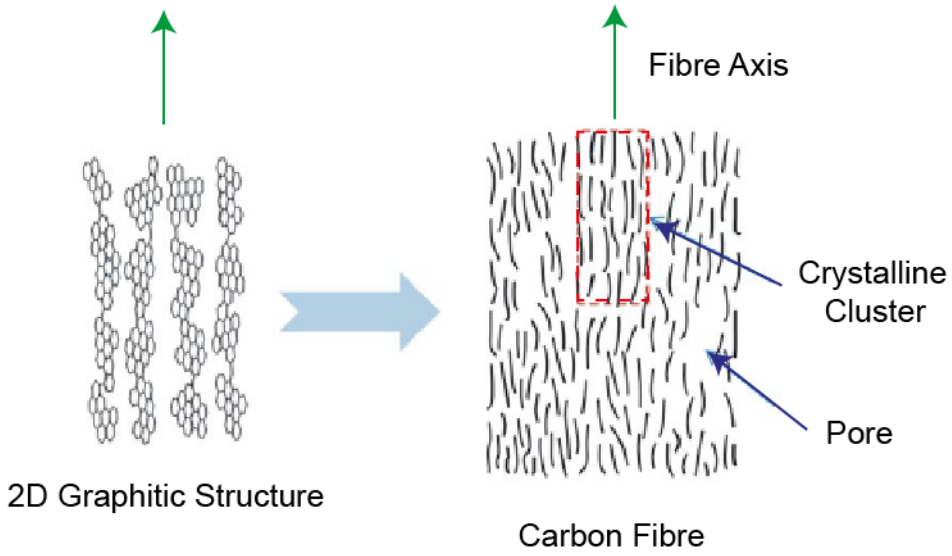

Figure 1: Schematic illustration of the basic structural model of carbon fibres.

This paper aims to develop a fundamental knowledge of the carbon fibre structure and morphology based on the development of a new synchrotron serial fibre X-ray scattering technique. Application of individual fibre measurements overcomes some of the common issues encountered with traditional fibre bundle scattering methods. The capacity to measure the mechanical and microstructure features at this length scale provides a new platform for the understanding of processing effects on carbon fibre. To demonstrate, three CF's with different processing tension were manufactured on the Carbon Nexus pilot scale carbonisation line.

2. EXPERIMENTATION

Carbonization line

Carbon fibre manufacture was conducted at Carbon Nexus, Deakin University on an industrial scale carbon fibre pilot plant equipped with a furnace from Despatch Industries, USA; and Furnace Engineering Pty Ltd, Australia). The facility has been optimized for the production of commercial grade CF at an industrial scale. A schematic of the manufacturing plant used for the production of the CF studied in this work is displayed in Fig. 2 .

Polyacrylonitrile (PAN) precursor fibres used in this study were acquired (12k tow) from Blue star Ltd, China. The PAN precursor was stabilized in oxidation ovens at temperatures between 230-260 °C. After further processing through the LT and HT furnaces the final carbonized fibre was obtained. Fiber processing conditions were based on a line speed of 120 m/h, a residence time in the stabilization ovens of 90 min, and 2.5min and 2.3 min in the LT and HT furnaces respectively. The average tension applied to the tow during oxidation was varied from 720 cN to 3030 cN. The low temperature and high temperature carbonization was held fixed at 1200 cN and 1700 cN respectively.

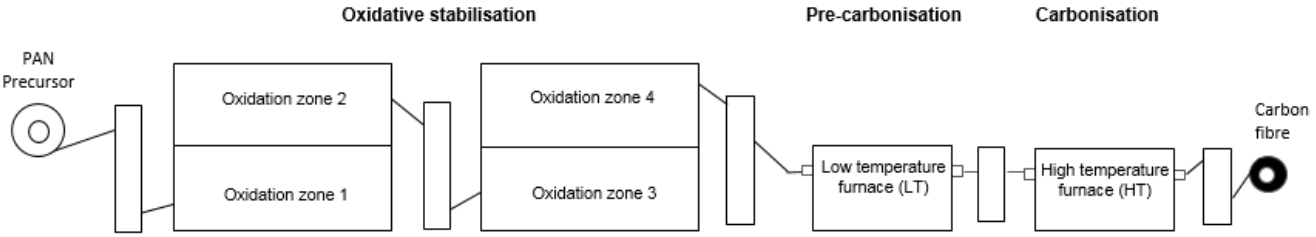

Figure 2: Pilot scale carbonization line at Carbon Nexus (Deakin University).

Mechanical testing on 50 CF's from each line tension was conducted using Favimat mechanical tester. The average results with tension according to low (720 cN), baseline (2300 cN) and high (3030cN) are reported in Fig. 3. As illustrated, the mean tension increase across the oxidation process led to a significant improvement in the fibre strength. The bars shown represent the standard deviation for the 50 fibres measured. Similarly, an improvement in fibre modulus was observed when the line tension was increased from 720 cN to 2300 cN while the modulus increase was only marginal from 2300 cN to 3030 cN.

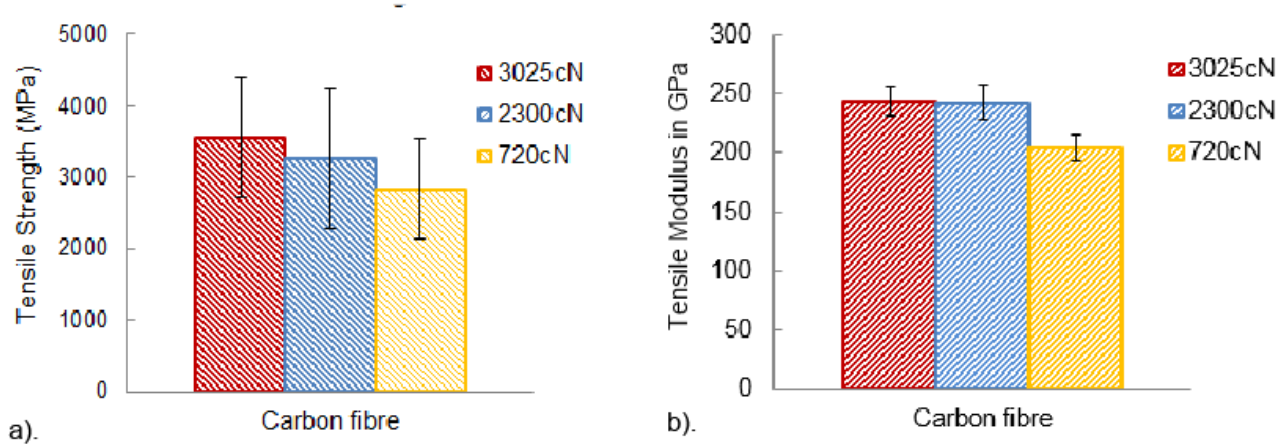

Figure 3: Mechanical testing results for CF's produced at slack, baseline and high processing tension.

Synchrotron serial fibre X-ray scattering

A new fibre specific scattering method has been developed on the SAXS-WAXS beamline at the Australian synchrotron facility (10). The beamline undulator and optics delivery system provides a highly collimated source of X-rays- beam size of ~30 μm (V) x 250 μm (H) at an X-ray flux of 10^{12} photons/s. Due to the weakly scattering nature of single CF's, the beamline was configured such that fibres were mounted in-vacuum. Figure 4a shows the necessary beamline modifications to achieve in vacuum SAXS-WAXS measurements. While Fig. 4b shows the vacuum high resolution linear stages and frame used to mount and scan each fibre, typically about 30 individual fibres are loaded onto a single frame. It should be noted, the entire end-station is currently undergoing an upgrade which will allow further improvements, including the addition of an in-vacuum detector and automated switching of camera length positions.

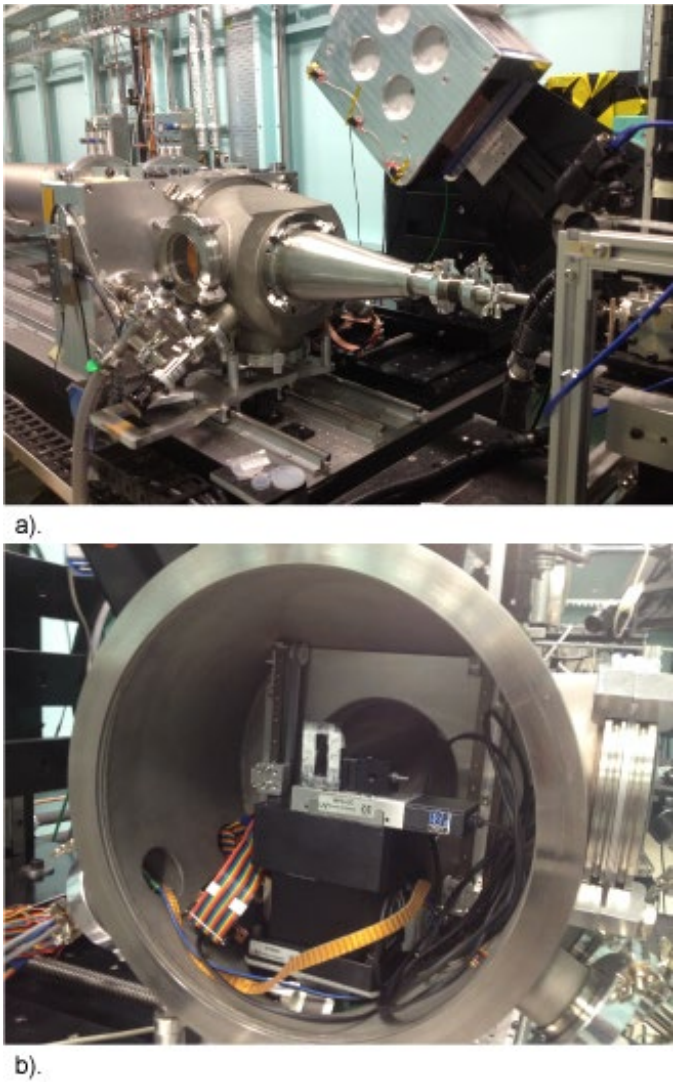

Figure 4: SAXS-WAXS end-station hardware design for serial fibre X-ray scattering measurements.

A summary of the data acquisition protocol and data reduction sequence is shown in Fig. 5. The challenge is to ensure each fiber is aligned with respect to the incident synchrotron X-ray probe. As the CF's were mounted with the fibre axis in the horizontal direction each fiber must be precisely aligned relative to the incident X-ray beam (30 μm FWHM in the vertical direction). A high resolution vertical translation stage was used to scan each fibre across the incident beam based on a step increment of 5 μm. Using a rapid exposure of 0.1 s individual frames were recorded as the fiber was scanned across - in total up to 100 exposures. A region of interest of the Pilatus 2D detector was selected to monitor the integrated intensity from the typical SAXS-WAXS CF pattern. In this instance the SAXS signal around the beamstop was monitored due to its high count rate. As the fiber passes through the central FWHM of the incident probe, the maximum integrated intensity and vertical stage position is stored. Once this scan is complete the fiber is moved back to the y-position and a longer (gapless) exposure is recorded, typically 10 s per detector position. For this work a single exposure was recorded for each CF so that data from 5 fibres per carbonization tension condition could be examined. All measurements were conducted at an energy of 15 keV and a camera length of 312.5 mm.

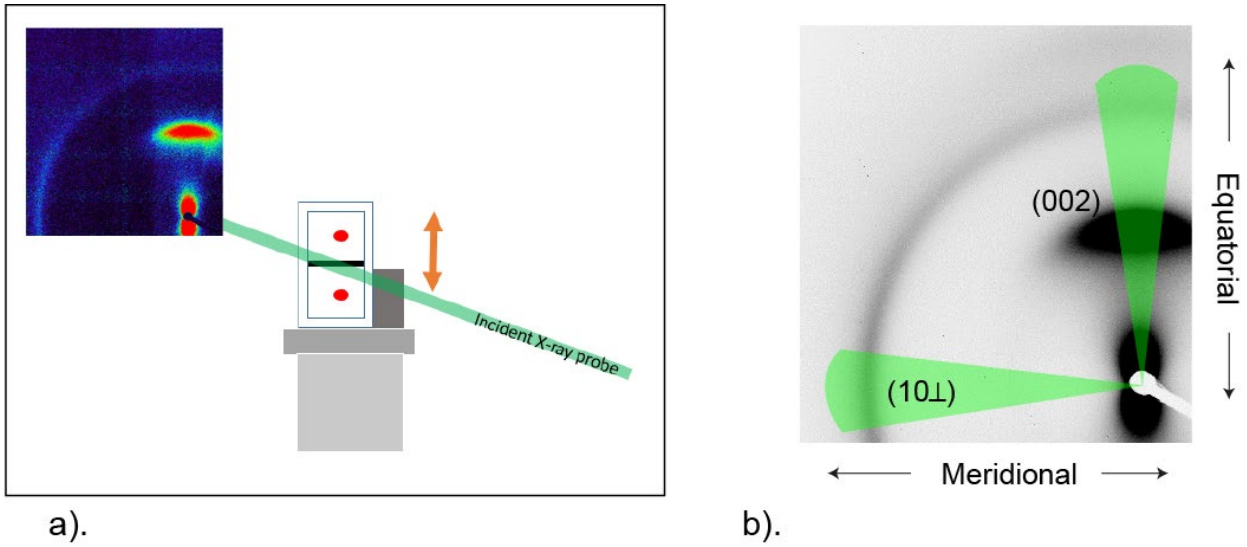

Figure 5: Schematic illustration showing the data acquisition and data reduction process.

As will be illustrated in the following discussion, single fibre measurements are highly sensitive to changes in the carbonization processing parameters. Experimental uncertainties are effectively reduced to a minimum, for example fibre misalignment commonly encountered in fibre bundle measurements is removed. As shown in Fig. 5b the characteristic SAXS-WAXS scattering pattern was observed with the WAXS (002) (equatorial direction) and (10⊥) (meridional direction) scattering arising from the preferred alignment of the 2D graphitic structure. Similarly the SAXS lobe type structure arising from the alignment of the porous structure is also clearly visible. For subsequent analysis of the SAXS-WAXS data, radial integration in both the equatorial and meridional direction was performed to quantify the fibre microstructural changes with line tension.

3. RESULTS

Identifying the microstructural properties responsible for driving CF mechanical performance is quite challenging as sufficient statistical insight requires a fibre-by-fibre analytical approach. Serial fibre scattering provides the necessary fidelity and ultimately with further refinement, datasets with improved statistical significance can be achieved. The subtle changes observed in the raw SAXS-WAXS images recorded for each fibre required careful line profile analysis. After radial integration of the WAXS data, line profile analysis was undertaken. Based on radial and azimuthal integration of the regions of interest defined in Fig. 5b, the X-ray specific profile fitting package Topas (11) was employed to extract precise peak information. The peak FWHM and 2θ position was obtained for both the (002) and (10 ⊥) reflections. This information was then used to assess the alignment, the size of the 2D graphitic sheets and the relative packing according to the CF processing tension applied.

Application of the azimuthal measurements was used to assess the degree of alignment of the 2D graphitic sheets relative to the fibre axis. The FWHM data for the (002) is displayed in Fig. 6. At the lowest tension of 720 cN the average degree of alignment ranged from 43.5 to 45.1 (ave: 44.3^{o}). As the process tension was increased to 2300 cN the degree of preferred alignment improved, ranging from 40.2 to 41.0 (ave: 40.6^{o}) and at the highest tension of 3025 cN a further slight improvement in the alignment was observed- from 38.5 to 40.6 (ave: 39.5^{o}). In the early studies of Youngs modulus in CF, Ruland (3) identified that the degree of preferred alignment was directly related to the modulus. This can be used to explain the impact of the observed change in azimuthal angle relative to the mechanical modulus results seen here. For example, at the carbonization tension of 720 cN the lowest modulus of ~200 GPa was observed. As the line tension increased to 2300 cN a significant modulus increase was observed and with a further increase in the line tension, a slight improvement in the modulus resulted. This is in direct agreement with the azimuthal angle results. At the lowest carbonization tension the level of preferred orientation, as defined by the azimuthal FWHM, is lowest ~44.3^{o}. Upon increasing the fibre processing tension to 2300 cN the degree of preferred alignment increased (~40.6^{o}) and finally as the line tension was increased to maximum (3030 cN) the preferred alignment only improved slightly to 39.5^{o}.

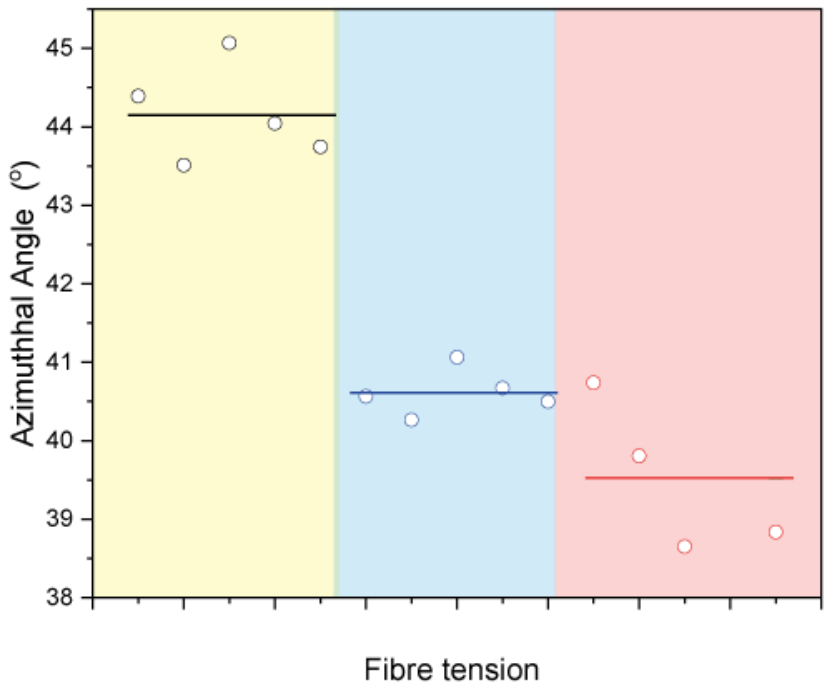

Figure 6: Summary of the (002) azimuthal FWHM data for 5 fibers analyzed at each line tension. The horizontal lines (black, blue, red) are used to represent the average values at each tension, 720 cN, 2300 cN and 3030 cN respectively.

The level of preferred orientation and hence fibre modulus driven by the change in processing tension reflects a change in the draw ratio of the fibers. As the applied tension decreases the draw ratio decreases. To identify the impact of the draw ratio on the fibre microstructure, in particular the impact on the packing of the 2D graphitic structure, measurement of the 2θ angle for both the (10⊥) and (002) was performed, these results are displayed in Fig. 7a and b respectively. For the (10⊥) data the low tension processing resulted in the highest 2θ value of ~20.690º (range 20.685º to 20.695º) and upon increasing the processing tension a systematic decrease in the 2θ position was observed. At a tension of 2300 cN the peak position dropped to 20.672º (range: 20.668º – 20.680º) with a further decrease observed at the highest tension of 3030 cN to 20.663º (range: 20.651º to 20.678º). Meanwhile the opposite trend with applied tension was observed for the (002). At 720 cN the smallest reading was recorded 12.167º (range: 12.158º to 12.176º). At a tension of 2300 cN the peak position increased to 12.190º (range: 12.185º – 12.198º) which increased further at the highest tension of 3030 cN to 12.206º (range: 12.198º to 12.211º).

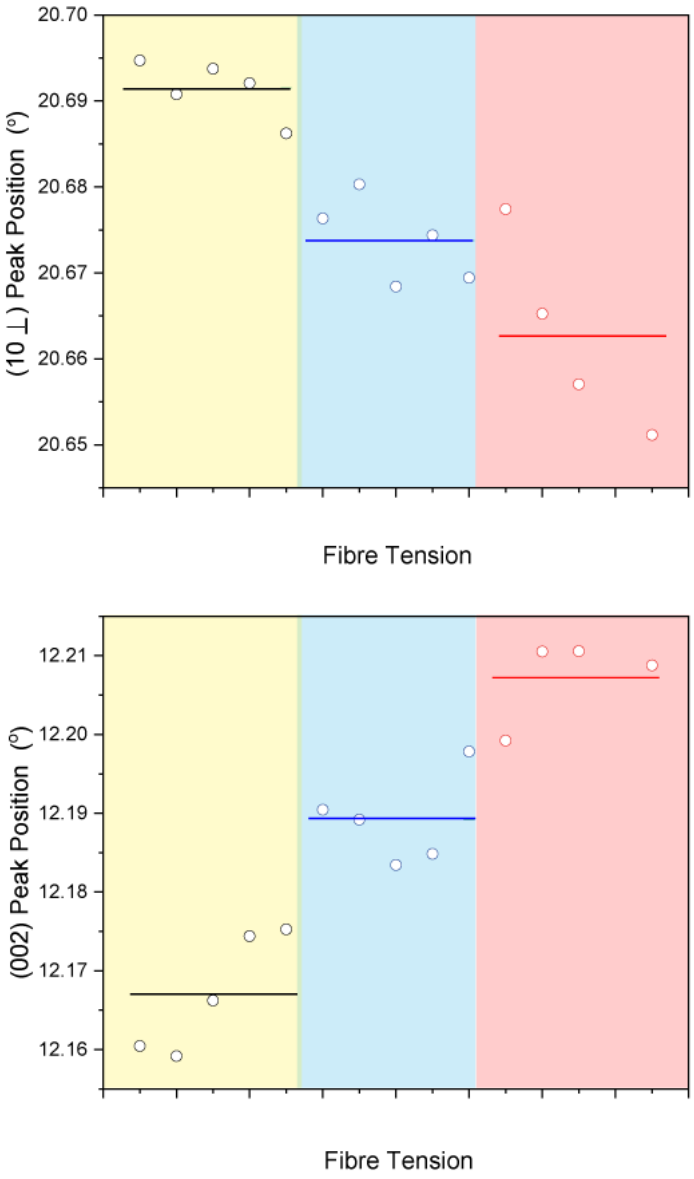

Figure 7: Summary of the 2q data for 5 fibers analyzed at each line tension for a). the (002) and b). (10⊥). The horizontal lines (black, blue, red) are used to represent the average values at each tension 720cN, 2300cN and 3025cN respectively.

This observed systematic change in the peak position for both the (10⊥) and (002) highlights the strong relationship of the alignment of the graphitic structure relative to the fibre tensile loading direction. As the tensile load is increased the atomic spacing of graphitic structure within the fibres responds accordingly. Since (10⊥) planes are oriented perpendicular to the loading direction, as the tension is increased the observed 2θ position decreases. Accordingly,

from Braggs law ($n\lambda = 2d\sin\theta$) the distance between atomic planes (lattice d-spacing) in the 2D structure increases with applied load. On the other hand, the (002) planes are oriented parallel to the loading direction. In this instance, as the tension increases the 2θ position increases (decrease in the d-spacing). i.e. as the tension increases this leads to tighter packing of the graphitic planes. Interestingly, the relative shift of the (10⊥) and (002) with applied tension is approximately the same order of magnitude which tends to signify the overall decrease in the diameter of the fibres with processing. Potentially the level of wrinkling of the graphitic structure with tension may have also reduced. Finally, as the (10⊥) increases with tension there may also be an elongation of the graphitic structure down the fibre axis.

After deconvolution of the instrument response, the broadening (FWHM) measured for both the (10⊥) and (002) was used to assess the change in the apparent crystallite size of the 2D structure with processing tension. According to the Scherrer equation, the size in a given crystallographic direction ($\langle t_a \rangle$) can be derived from the measured broadening (β) according to $\langle t_a \rangle = 0.9\lambda/\beta\cos\theta$. Where λ is the X-ray wavelength and θ is the Bragg scattering angle. Results for both the (10⊥) and (002) are shown in Fig. 8. Again a clear trend can be identified according to the change in applied tension during oxidation. In both directions a small but steady increase is observed. For (10⊥) the apparent crystallite size increased with tension from 2.38 nm to a maximum of 2.43 nm while the (002) increased from 1.70 nm to 1.79 nm. Although the observed changes are slight, a change in aspect ratio of the crystallites is seen. Interestingly, this observed increase in elongation along (10⊥) with applied load and subsequent fibre mechanical properties is in agreement with recently proposed Eshelby's based model developed to understand the anisotropy strengthening in CF (Tane et al, 2019). In this instance the increased level of connectedness of the graphitic structure down the fibre axis was found to be responsible for driving the fibre modulus and anisotropy.

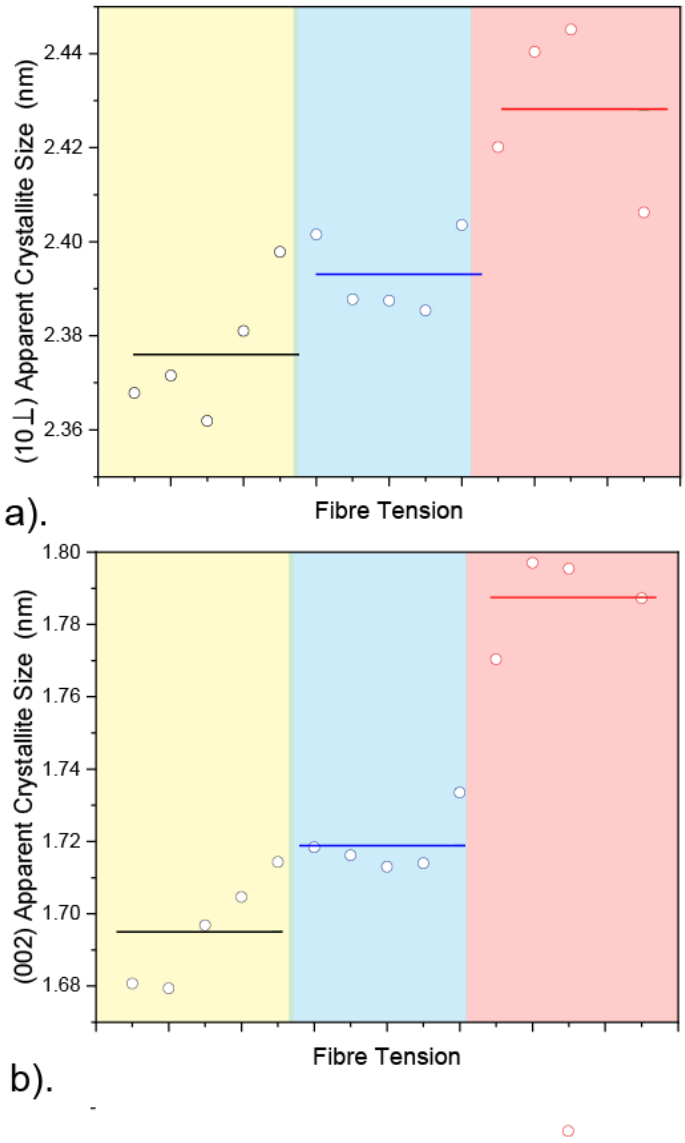

Figure 8: The measured crystallite size evolution according to the change in fibre tension for a). (10⊥) and b). (002). Again black, blue and red horizontal lines reflect the average results for carbonization tensions of 720cN, 2300cN and 3025cN respectively.

As illustrated in Fig. 5b the raw scattering data displayed the characteristic lobe type SAXS pattern commonly observed in PAN derived CF. To understand the role of carbonization tension on the SAXS signal, the distribution and size of the pores was evaluated according to the Ruland method (12). The tangential width of the equatorial SAXS distribution (β_{eq}) is plotted against q^2 in Fig. 9. For display purposes only, results for a single fibre at each oxidation tension are shown. A linear fit was used to study the subtle differences observed from each fibre. The intercept results indicated that the change in pore width decreased with tension; 7 nm at 720 cN,

6.6 nm at 2300 cN and 5.1 nm at 3030 cN. The increase in tension also resulted in a sharpening of the pore orientation relative to the fibre axis. Ranging from 24° at 720 cN decreasing to 22° at 2300 cN and finally 21° at the maximum applied load of 3030 cN.

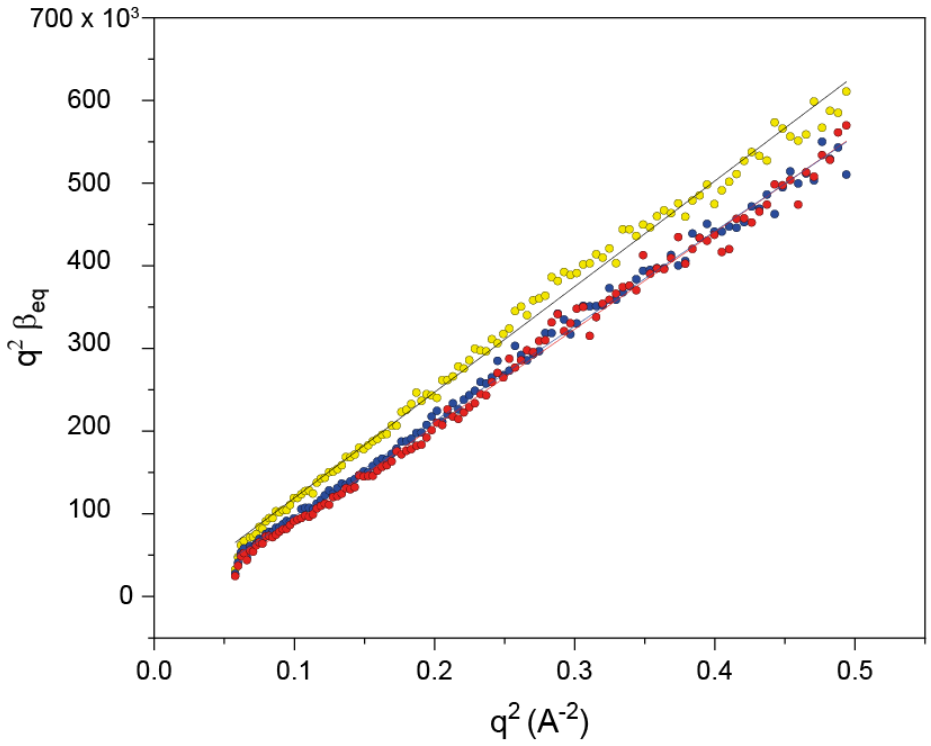

Figure 9: Plot of the equatorial distribution of the SAXS signal against q^2 and corresponding linear fits for the carbonized fibres at tensions of 720 cN (yellow fibre3), 2300 cN (blue fibre 3), and 3030 cN (red fibre 3).

4. CONCLUSIONS

The application of serial fibre X-ray scattering was used to identify the key microstructural features leading to the change in CF mechanical properties as carbonization line tension was varied. The main findings included,

1. As oxidization fibre tension increased from 720 cN to 300cN an increase in the CF modulus was identified. This also led to an improvement in the alignment of the graphitic structure relative to the fibre axis with an accompanying increase in the size of the 2D graphitic structure in the fibre.

2. An increase in the oxidization fibre tension led to an increase in the 2D packing, as observed by an increase in the 2θ position of the (002) of the graphitic structure. This tension also served to increase the spacing in the graphitic structure (10 ⊥) parallel to the loading axis.

3. Finally, the fibre tension also appears to reduce the width and alignment of the pores which may be responsible for the observed improvement in the tensile strength of the fibre.

Overall the structural property information appears to follow a clear trend. However, efforts are currently underway to improve the sample statistics which will build greater confidence in the observed outcomes.

5. ACKNOWLEDGEMENTS

All X-ray scattering measurements were undertaken on the SAXS/WAXS beamline at the Australian Synchrotron (Victoria).

6. REFERENCES

1. Chand, S. J. ‘Review Carbon fibres for composites’. (2000). *J. Mat. Sci*. 2000, 35, Pp. 1303- 1313. doi.org/10.1023/A:1004780301489.
2. Oberlin, A. ‘Carbonization and Graphitization’. (1984). *Carbon*, 22, 6. Pp. 52I-541.
3. Ruland W. ‘The relationship between preferred orientation and Young's modulus of carbon fibers’. (1969), *Appl. Polym. Symp*. 9:293- 301.
4. Northolt M. G, Veldhuizen H. L, Jansen H. ‘Tensile deformation of carbon fibers and the relationship with the modulus for shear between the basal planes’. *Carbon* (1991), 29(8), Pp. 1267- 1279.
5. D. Loidl, D. O. Paris, O. Burghammer, M. Riekel, C. Peterlik, H. ‘Direct Observation of Nanocrystallite Buckling in Carbon Fibers under Bending Load’. *Phys. Rev. Lett.* 2005, 95, 225501-4. Doi: 10.1103/PhysRevLett.95.225501.

6. M.Tane, M. Okuda, H. Tanaka, F. ‘Nanocomposite microstructures dominating anisotropic elastic modulus in carbon fibers’. *Acta Mat*. (2019), 166, Pp. 75-84. https://doi.org/10.1016.
7. Griffith, A. A. ‘The phenomena of rupture and flow in solids’. *Phil. Trans. Royal Society London,* A, (1921), 221, Pp. 582–593. doi*:*10.1098/rsta.1921.0006.
8. Dieter Loidl, D. Paris, O. Rennhofer, H., Muller, M. Peterlik, H. ‘Skin-core structure and bimodal Weibull distribution of the strength of carbon fibers’. (2007), *Carbon*, 45. Pp. 2801–2805. doi:10.1016/j.carbon.2007.09.011.
9. Li, D. Lu, C, Wu, G., Hao, J. Yang, Y. Feng, Z., Li, X. Ana, F. Zhang, B. ‘Structural evolution during the graphitization of polyacrylonitrile-based carbon fiber as revealed by small angle X-ray scattering’. (2014). *J. Appl. Cryst.* 47, 1809–1818. doi:10.1107/S1600576714020081.
10. Kirby, N. M. Mudie, S. T. Hawley, A. M. Cookson, D. J. Mertens, Cowieson, Samardzic-Boban, V. ‘A low-background-intensity focusing small-angle X-ray scattering undulator beamline’. (2013). J. Appl. Cryst. 46, Pp. 1670–1680. *J. Appl. Cryst.* (2013). https://doi.org/10.1107/S002188981302774X.
11. Bruker. TOPAS, Total Pattern Analysis Solutions, Bruker-AXS, Madison, WI, 2005.
12. Thunemann, A. F. Ruland, W. ‘Lamellar Mesophases in Polyacrylonitrile: A Synchrotron Small-Angle X-ray Scattering Study’. (2000), *Macromolecules***,** 33, Pp. 2626-2631.